Nanoscale

PAPER

View Article Online
View Journal | View Issue

Check for updates

Cite this: *Nanoscale*, 2022, **14**, 14223

Nanoceria dissolution at acidic pH by breaking off the catalytic loop†

Dmitry Galyamin, [a] Lena M. Ernst,[b] Aina Fitó-Parera,[a] Guillem Mira-Vidal, [c] Neus G. Bastús, [c] Neus Sabaté *[a,d] and Victor Puntes *[b,c,d]

Received 30th June 2022,
Accepted 11th August 2022

DOI: 10.1039/d2nr03586c

rsc.li/nanoscale

This manuscript proves the reproducibility and robustness of cerium oxide nanoparticles, nanoceria, employed as a chemical reagent with oxidizing capacity (as an electron sink) at acidic pH. Unlike nanoceria multi-enzyme-mimetic capabilities at neutral or high pH, nanoceria can behave as a stoichiometric reagent at low pH where insoluble Ce^{4+} ions transform into soluble Ce^{3+} in the nanocrystal that finally dissolves. This behaviour can be interpreted as enzyme-like when nanoceria is in excess with respect to the substrate. Under these conditions, the Ce^{3+}/Ce^{4+} ratio in the NPs can easily be estimated by titration with ferrocyanide. This procedure could become a rapid assessment tool for evaluating nanoceria capacity in liquid environments.

Open Access Article. Published on 19 August 2022. Downloaded on 7/19/2025 7:26:35 AM.
This article is licensed under a Creative Commons Attribution-NonCommercial 3.0 Unported Licence.

Introduction

Having the benefits of low cost, excellent stability and tolerance to extreme conditions, inorganic nanoparticles (NPs) have revealed promising features that make them reliable and robust alternatives to natural enzymes. Since the peroxidase-like activity of magnetite (Fe_3O_4) NPs was first described in 2007,[1] there has been exponential growth of studies on enzyme-like NPs, also called nanozymes,[2,3] not without controversy.[4] Among them, nanoceria, cerium oxide (CeO_2) NPs, is of particular interest due to its observed multi-enzyme-mimetic capabilities, including antioxidant activity, such as in superoxide dismutase (SOD)[5] and catalase,[6,7] and pro-oxidant activity such as in peroxidase.[8,9] Asati and co-workers recently reported nanoceria activity as an oxidase-like enzyme under mildly acidic conditions.[10] These nanoceria multi-enzyme-like properties have been successfully used for biological detection, substituting the widely used HRP enzyme with a more robust and reliable alternative.[11] Additionally, nanoceria ability to scavenge excess reactive oxygen species (ROS) in living cells has popularized studies for its application as an anti-inflammatory substance.[12]

The mechanism responsible for the reported behaviour arises from the ability of Ce atoms to adjust their electronic configuration to best fit their immediate electromagnetic environment. The main difference between rare earth and other metals is having 4f orbitals, whose electrons are shielded by 4d and 5p orbitals. This orbital shield makes 4f electrons weakly bond to the nucleus allowing Ce ions to easily switch between Ce^{3+} and Ce^{4+} valence states, creating oxygen vacancies compensating for the positive charge deficiency. This phenomenon is particularly strong at the nanoscale, where the very high surface-to-volume ratios withstand a significant concentration of oxygen vacancies at the NP surface accompanied by cerium ions reduced to the Ce^{3+} state.[13] In this redox process, the fluorite (fcc) structure of the crystal is maintained, facilitating the oxidation of Ce^{3+} ions back to Ce^{4+} ions and thus enabling the regenerative ability of nanoceria to act catalytically.[12] The precise amount of oxygen vacancies and cerium atoms in the Ce^{3+} state in the NPs increases with a decrease in size,[14,15] and can be modified by the synthesis method.

This work explores the conditions where this catalytic loop is broken and Ce^{3+} ions are not oxidized back to Ce^{4+}. Systematic experiments evidenced that under the working conditions (at low pH), nanoceria behave as a pure stoichiometric reagent consumed during the reaction. However, this behaviour can be interpreted as enzyme-like when the substrate undergoing oxidation is the limiting reagent, not the nanoceria. Interestingly, under such conditions, unlike enzymes, a limiting reagent can stop the "enzymatic" analytical reaction at the desired reading point, facilitating detection.

[a]*Instituto de Microelectrónica de Barcelona, IMB-CNM (CSIC). C/dels Til·lers, Campus Universitat Autònoma de Barcelona (UAB), 08193 Barcelona, Spain. E-mail: neus.sabate@imb-cnm.csic.es*
[b]*Vall d'Hebron Research Institute (VHIR). Hospital Universitari Vall d'Hebron, Passeig de la Vall d'Hebron, 129, 08035 Barcelona, Spain. E-mail: victor.puntes@icn2.cat*
[c]*Institut Català de Nanociència I Nanotecnologia (ICN2), CSIC and The Barcelona Institute of Science and Technology (BIST). Campus UAB, 08193 Barcelona, Spain*
[d]*Institució Catalana de Recerca I Estudis Avançats (ICREA), 08010 Barcelona, Spain*

† Electronic supplementary information (ESI) available. See DOI: https://doi.org/10.1039/d2nr03586c

Open Access Article. Published on 19 August 2022. Downloaded on 7/19/2025 7:26:35 AM.
This article is licensed under a Creative Commons Attribution-NonCommercial 3.0 Unported Licence.

Results and discussion

Nanoceria of ~3 nm diameter at a concentration of 1.72 mg ml^{-1} (1.6×10^{16} NPs ml^{-1}) was synthesized using a hydrothermal approach with sodium citrate as a complexing and stabilizing agent. Sodium citrate, a tricarboxylic acid with three pKa values (3.06, 4.74, and 5.4), provides electrostatic stabilization to the NPs at a pH value higher than 3.5, creating an electrostatic stable colloidal solution, as the surface charge *vs.* pH measurements indicate (Fig. S1†). Morphological characterization by high-angle annular dark-field scanning transmission electron microscopy (HAADF-STEM) reveals the formation of non-aggregated 2.9 ± 0.8 nm quasi-spherical nanoceria particles of high uniformity and narrow diameter distribution (Fig. 1A). The hydrodynamic diameter was measured by dynamic light scattering (DLS) (Fig. 1B), obtaining a monomodal distribution peaking at 4.5 ± 0.2 nm (PDI = 0.26). The zeta potential (Fig. 1C) shows that NPs, after purification and resuspension in 2.2 mM SC, are negatively charged (−47.6 mV at pH = 9.36 and conductivity = 0.24 mS cm^{-1}), which can be ascribed to the citrate molecules reversibly adsorbed onto the NP surface. This reversibility is easily proven under dialysis conditions, where, as the citrate concentration decreases, the NPs aggregate (data not shown). The X-ray diffraction patterns of the as-synthesized nanoceria confirm that the sample displays a pure single-phase fluorite (face-centred cubic, fcc) structure (JCPDS No. 34-0394). The diffraction peaks are substantially broadened, reflecting the ultra-small crystal size (Fig. 1D). In Fig. 1E, the UV-visible spectrum of nanoceria shows a distinct absorption band at 282 nm, which, following Tauc plot, reveals an optical band gap of 3.06 eV. As catalysis is a surface phenomenon, the colloidal stability of nanoceria during experiments is critical. Aggregation would lead first to a dramatic reduction of the total exposed NP surface and then to the NP precipitation out of the reaction mixture. The colloidal stability of nanoceria in the working media was measured as a function of time (Fig. 1F). The spectra do not show any significant aggregation or sedimentation, indicating the colloidal and chemical stability of the NPs under experimental conditions, at pH 4,4, where oxidase-like nanoceria capacity has been described.[10]

In this work, we characterize nanoceria evolution during the water oxidation process of ferrocyanide ($[Fe(CN)_6]^{4-}$) to ferricyanide ($[Fe(CN)_6]^{3-}$) at pH 4.4 as a model of redox colourimetric reaction.[10] Typical species employed as redox mediators in these enzymatic-type reactions are organic dyes such as 3,3′,5,5′-tetramethylbenzidine (TMB), 2,2-azinobis(3-ethylbenzothizoline-6-sulfonic acid) (ABTS), and dopamine (DOPA).[10] These dyes feature high molar extinction coefficients (ε), allowing high sensitivity on optical measurements at low reagent

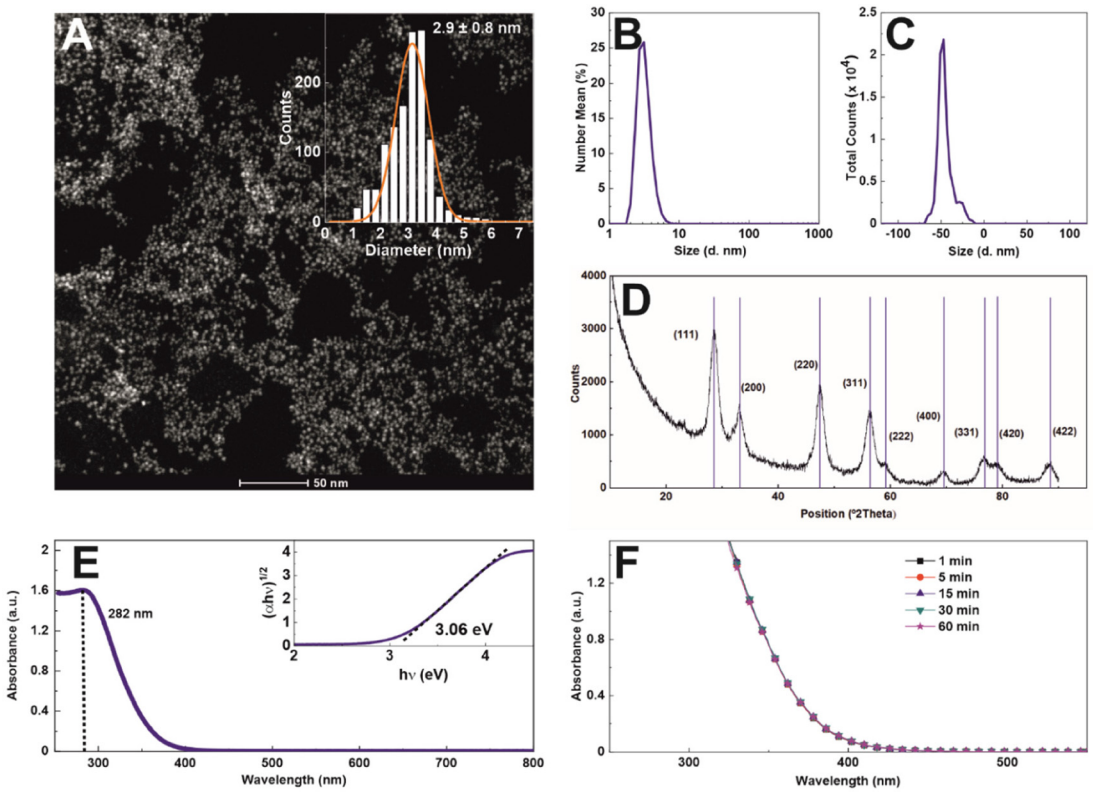

Fig. 1 Synthesis and characterization of nanoceria. (A) HAADF-STEM images of the as-synthesized NPs. Size distribution (inset). (B) Hydrodynamic profile measured by dynamic light scattering. (C) Zeta potential analysis. (D) X-ray diffraction pattern of the as-synthesized nanoceria and JCPDS No. 34-0394 standards. (E) The UV-visible spectrum of the nanoceria and optical bandgap energy determination using the Tauc equation (inset). (F) Colloidal stability of nanoceria dispersed in the working citrate buffer (100 mM, pH 4.4).

This journal is © The Royal Society of Chemistry 2022

Open Access Article. Published on 19 August 2022. Downloaded on 7/19/2025 7:26:35 AM.
This article is licensed under a Creative Commons Attribution-NonCommercial 3.0 Unported Licence.

concentrations. However, the optical signal saturates approximately at relatively low concentrations for similar reasons, which restricts kinetic studies (time evolution as a function of enzyme *vs.* dye ratio) to minimal concentration ranges. Because of that, we choose to employ transparent ferrocyanide and its redox pair, yellow-coloured ferricyanide (absorbance peak at ~420 nm), as a redox mediator.[16] As ferricyanide presents a much lower ε value than most organic dyes used in the field (see Table S1 ESI†), it allows for directly measuring a broader range of nanoceria/ferrocyanide concentration ratios before spectral saturation, allowing for easy reaction kinetics follow-up.

The performance of nanoceria for the oxidation of a solution of 1 mM ferrocyanide was evaluated at five different nanoceria concentrations, ranging from 8.1×10^{-3} to 1.62×10^{-1} mg mL^{-1} (4.7×10^{-2} to 9.4×10^{-1} mM atomic cerium in the form of nanoceria). In these experiments, ferrocyanide is first added to a cuvette and then nanoceria to initiate the reaction. In our experiments, the pH of the solution was adjusted at pH = 4.4 (citrate buffer 100 mM) following previous studies that revealed this one as an optimal pH for nanoceria oxidase-like behaviour.[10] As soon as both species mix, a yellow color appears in the transparent solutions evidencing the chemical reaction progression and the formation of ferricyanide. The temporal evolution of the UV-vis absorption spectra is shown in Fig. 2A, where an increase in intensity until saturation after 3 hours of reaction can be observed. In Fig. 2B it is shown how the final ferricyanide peak intensity depends on the initial nanoceria concentration, suggesting that nanoceria is acting as a limiting reagent, rather than a catalyst, in a first-order reaction, with a rapid increase of conversion at short times that evolves towards a saturation point and a plateau as it is consumed (Fig. 2C). Under the same experimental conditions, the ferrocyanide oxidation process was compared with laccase enzyme, from the phenol oxidise group enzymes, at the same mass concentration (1.62×10^{-4} mg mL^{-1}) (Fig. 2C). Contrary to nanoceria, laccase displays a linear time-dependent behaviour and a constant reaction rate, consistent with its widely reported catalytic activity.

If we look at the cerium oxide signal in the UV-vis spectra now, we also see how it does transform during this process. Fig. 3A shows the recorded spectra after adding 0.47 mM atomic cerium (in the form of nanoceria) to a solution containing ferrocyanide in excess (1 mM). The strong absorption signal has well-defined features in the near-ultraviolet region (>400 nm), accounting for the presence of nanoceria.[17] As the reaction proceeds, the intensity of this band diminishes while the characteristic band of ferricyanide arises. These features can be attributed to a change in the cerium oxidation state, from Ce^{4+} to Ce^{3+} (Ce^{4+} = 320 nm, Ce^{3+} = 253 and 295 nm)[18] while ferrocyanide gets oxidized, as nanoceria is consumed. We repeated the same experiments with a batch of commercial nanoceria of similar diameter to test whether the process is consistent and independent of nanoceria synthetic conditions. Fig. 3B shows the initial and final spectra of both the in-house and commercial nanoceria. Due to the similar concentration of nanoceria solutions, the initial spectra for both nanomaterials (dashed lines) superimpose. However, at the end of the reaction, the decrease of the UV-vis absorption spectra at low wavelengths was more evident when commercial nanoceria was employed. These results suggest that the in-house nanoceria present higher oxidation capacity than the commercial ones (less ceria is consumed), which can be attributed to a lower Ce^{3+} concentration in the original NPs (see below).[19]

As the reaction of cerium to iron is one to one (eqn (1)), one would expect a stoichiometry of 1:

$$CeO_2 + 4H^+ + [Fe(CN)_6]4^- \rightarrow Ce^{3+} + 2H_2O + [Fe(CN)_6]^{3-} \quad (1)$$

However, as the amount of Ce^{4+} in the NPs is less than the total amount of Ce ions, due to oxygen vacancies, we titrated nanoceria with ferrocyanide to determine the actual Ce^{4+} concentration in the NPs.

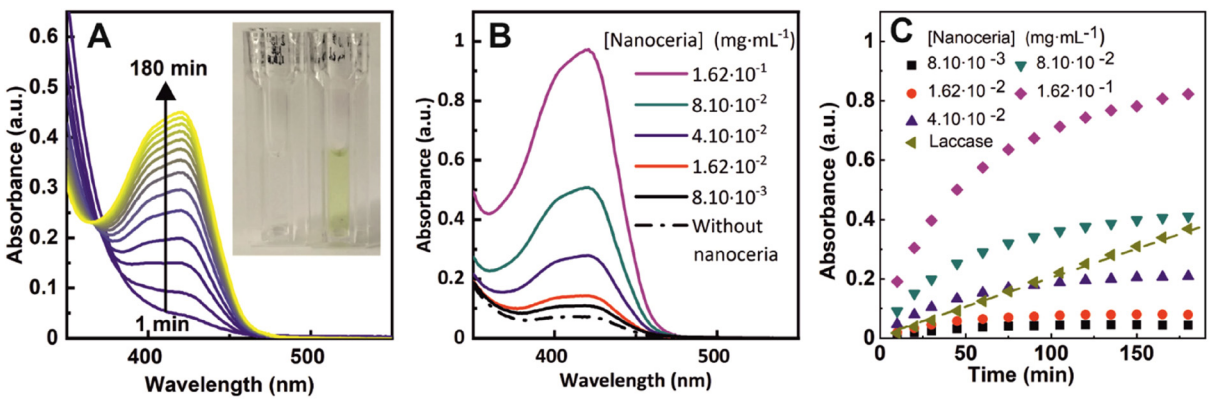

Fig. 2 (A) UV-vis spectra of 1 mM ferrocyanide solution exposed to 8.1×10^{-2} mg mL^{-1} (4.7×10^{-1} mM total atomic cerium) nanoceria for 180 min Spectra were recorded every 15 min for 3 hours. (B) Final UV-vis spectra (at 24 h) of the 1 mM ferrocyanide solution exposed at different nanoceria concentrations. (C) and (A) Absorbance values at 420 nm for 1 mM ferrocyanide solutions exposed to different nanoceria concentrations, ranging from 8.10×10^{-3} mg mL^{-1} to 1.62×10^{-1} mg mL^{-1} (0.047 to 0.94 mM) and to laccase at a concentration of 1.62×10^{-4} mg mL^{-1} for 180 minutes.

Open Access Article. Published on 19 August 2022. Downloaded on 7/19/2025 7:26:35 AM.
This article is licensed under a Creative Commons Attribution-NonCommercial 3.0 Unported Licence.

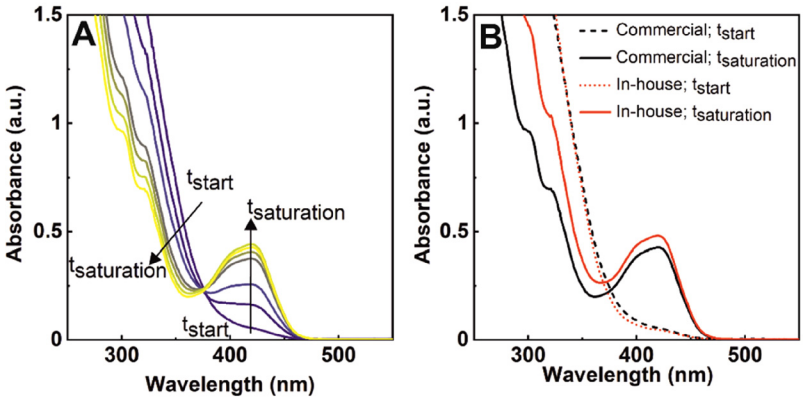

Fig. 3 (A) Absorbance spectra of 1 mM ferrocyanide solution exposed to nanoceria at a concentration of 8.10 × 10^{-2} mg mL^{-1} (0.47 mM) for 60 minutes, (B) comparison of UV-vis spectra between commercial and in-house nanoceria at t = 0 min and after 60 min of reaction.

We prepared a set of commercially and in-house synthesized nanoceria solutions and fixed the nanoceria content to 0.4 mg mL^{-1} (2.3 mM atomic cerium). Additional solutions with 0.5 mg mL^{-1} laccase enzymes coming from different batches were also prepared for comparison. The solutions were mixed with ferrocyanide solutions of varying concentrations, ranging from 0 to 2.4 mM, and allowed to react until the ferrocyanide was entirely consumed. Fig. 4 shows the values of the absorption intensity at 420 nm for both enzymatic and nanoceria preparations. As expected, when the ferrocyanide content is low (0 to 1.5 mM), all concentrations tested show a linear behavior between the initial ferrocyanide content and absorption intensity at saturation, indicating that all the ferrocyanide has been oxidized. At these concentrations, the enzyme performance also superposes that linear dependence. At higher ferrocyanide concentrations, nanoparticles cannot further increase the signal at 420 nm while laccase linearly does it. Taking into account that nanoceria at 0.4 mg mL^{-1} corresponds to a concentration of atomic cerium of approximately 2.3 mM, the ferrocyanide oxidation capacity of these nanoceria solutions could be estimated to be around 1.65 mM. This corresponds to a NP with about 36% of Ce^{3+} similar to what is obtained from XPS (Fig. S2†) and it is consistent with the small NP diameter, the large surface to volume ratio and the corresponding accumulation of oxygen vacancies.

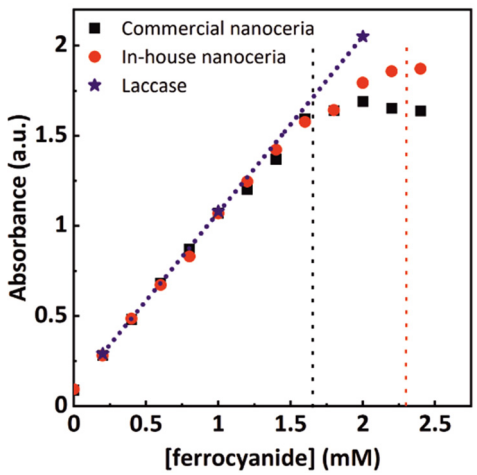

Fig. 4 Absorbance values at 420 nm after 60 minutes for a set of solutions with a fixed concentration of 0.4 mg mL^{-1} (equivalent to 2.3 mM atomic cerium) for commercially and in-house synthesized nanoceria and different initial concentrations of ferrocyanide, ranging from 0 to 2.4 mM. Spectra between commercial and in-house nanoceria at t = 0 min and after 60 min of reaction.

Under these conditions, Ce^{4+} atoms in nanoceria act as electron acceptors oxidizing the molecules of interest. In nanoceria, the formed Ce^{3+} ions can easily be oxidized again back to Ce^{4+}, closing the catalytic loop. However, following the Pourbaix diagram,[20] cerium atoms in water thermodynamically prefer to remain in the Ce^{3+} oxidation state at acidic pH. In this case, the catalytic loop can be broken, and nanoceria behaves as a stoichiometric reagent where Ce^{4+} transforms into Ce^{3+} in the NPs that finally dissolves, as previously reported in plant growth media.[21] Accordingly, after nanoceria consumption, no NPs were observed by TEM after exhaustive analysis of the sample grid, neither a nanoceria DLS nor UV-vis signal (data not shown). To look closer at nanoceria evolution during ferrocyanide oxidation, DLS and ICPMS measurements were performed before and after incubation of ferrocyanide and nanoceria at different ratios for 3 hours. 2.35 mM atomic cerium in the form of nanoceria was exposed to increased concentrations of ferrocyanide (0.77, 1.16, 1.54 and 2.3 mM). DLS and the corresponding NP concentration analyses show the progressive dissolution of the NPs maintaining the NP number rather constant until disintegration at high ferrocyanide concentrations (Fig. 5A).

For ICPMS analysis, the samples were purified by centrifugation–filtration before analysis to separate NPs from cerium ions. Fig. 5C shows how the presence of Ce^{3+} ions in solution increases as the amount of ferrocyanide increases. The discrepancy between the expected and elemental measured values is attributed to some retention in the purification filters and the spontaneous oxidation of ferrocyanide during the experimental time window.

 This journal is © The Royal Society of Chemistry 2022

Open Access Article. Published on 19 August 2022. Downloaded on 7/19/2025 7:26:35 AM.
This article is licensed under a Creative Commons Attribution-NonCommercial 3.0 Unported Licence.

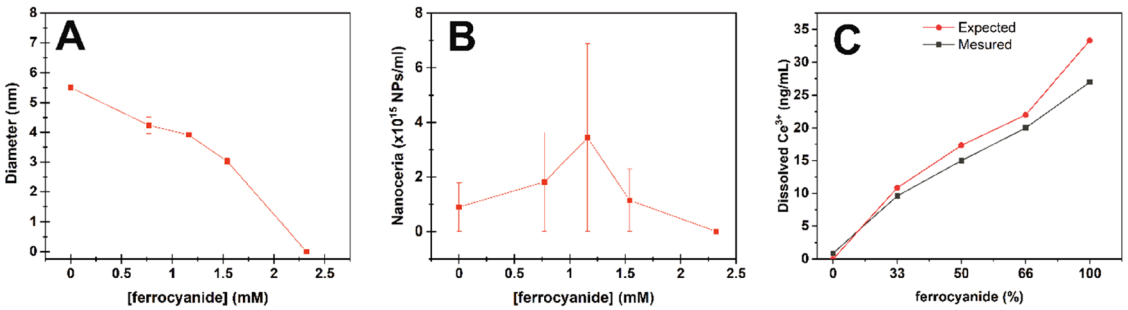

Fig. 5 In-house synthesized cerium NPs at a concentration of 0.4 mg ml^{-1} (equivalent to 2.3 mM atomic cerium) reacting for 3 hours with different concentrations of ferrocyanide, ranging from 0 to 2.4 mM. (A) Hydrodynamic diameter by intensity profiles measured by DLS plotted against $K_4[Fe(CN)_6]$ concentrations. (B) CeO_2 NP concentrations measured by DLS. (C) Dissolved cerium ions measured by ICPMS, plotted against $K_4[Fe(CN)_6]$ concentrations.

This translates into nanoceria being able to uptake a finite number of electrons while maintaining its fluorite crystal structure and NP integrity before disintegration. Note that Ce^{3+} ions are soluble in water. Therefore, if Ce^{3+} ions and the corresponding oxygen vacancies are not recycled back to Ce^{4+} and oxygen absorbed, the increasing concentration of these oxygen vacancies in the NPs will lead to cation repulsion and irreversible disintegration of the NPs. Despite that, it is well known that the dissolution of cerium oxide in aqueous solutions is hindered by the great stability of the crystalline network, the same that endures the cyclic formation of oxygen vacancies and cerium reduction.[22] However, nanoceria around 2–3 nm is very close to the calculated thermodynamically stable crystal size[23] facilitating NP dissolution. This process accelerates as pH decreases. We did control experiments where nanoceria was incubated at pH 4.4 and pH 1.7 (Fig. S3†). In the absence of ferrocyanide, a good electron source, the NP dissolution takes about 60 hours, while at pH 1.7, it takes less than 3 hours.

Finally, when comparing inorganic nanoparticles and biological enzymes, reproducibility and robustness have largely been described as features that make NPs desirable candidates to substitute enzymes. We evaluated these two aspects with two different batches of laccase enzymes and the two different ceria NPs (in-house and commercial NPs) tested under the same conditions (Fig. 6A). It can be seen that while enzymes show very different oxidation rates per mass, the nanoceria data superimposes. This difference in response between enzymes is a widespread phenomenon as the complexity of calculating the activity per mass of protein itself, which is highly variable. Another interesting feature of nanoceria is that, unlike enzymes, it does not require any specific storage conditions or handling. A batch of in-house synthesized nanoceria solutions was stored at room temperature and under ambient light exposure for one month. Ferrocyanide oxidation measurements were performed on days 1, 15, and 30 for the five tested concentrations. The results are shown in Fig. 6B. The nanoceria oxidative capability remains unaltered (p < 0,05),

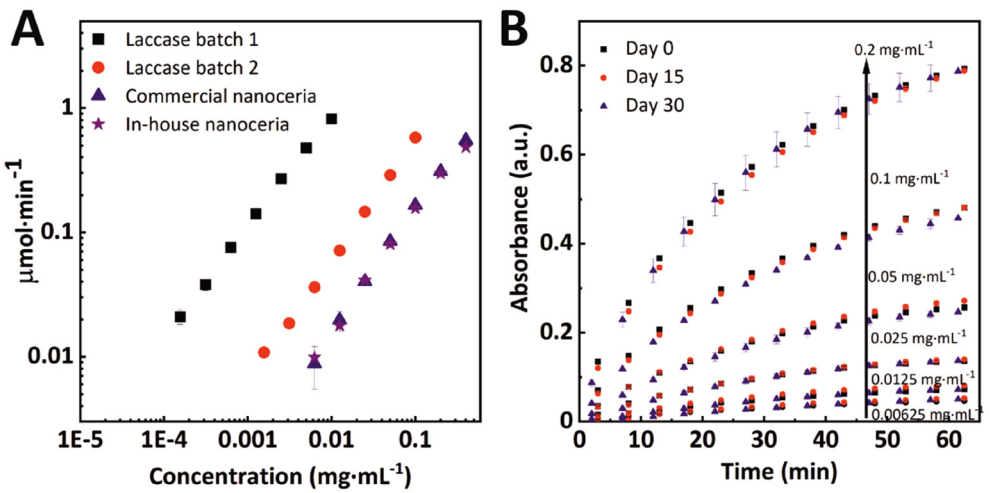

Fig. 6 (A) Oxidation reaction rate for different concentrations of two different batches of laccase, commercial and in-house nanoceria in the presence of 1 mM ferrocyanide. (B) Absorbance measurements for the in-house batch of nanoceria for over a month (n = 3). The results show remarkable reproducibility and statistically non-significant differences (p < 0.05).

Open Access Article. Published on 19 August 2022. Downloaded on 7/19/2025 7:26:35 AM.
This article is licensed under a Creative Commons Attribution-NonCommercial 3.0 Unported Licence.

showing robustness under low demanding storage conditions. For larger storage times, we recommend doing it in the dark to avoid citrate sodium degradation.

Several works have described the mode of action of nanoceria, sometimes reaching contradictory conclusions about its catalytic nature. Variability in pH has been proved to be one of the most relevant parameters directly influencing nanoceria activity.[10,24] For instance, nanoceria presents excellent antioxidant capacity in water at neutral or high pH, while oxidative capacities of nanoceria have been observed preferably under acidic conditions, at pH 4 to 6.[10,24] Yang and co-workers attempted to elucidate the pH-dependent oxidizing mechanism and the role of oxygen in the reaction,[25] while presenting mixed articles reporting both catalytic-like and reagent-like activity.

Conclusions

The association of the redox activity of nanoceria as a reagent or a catalyst is not straightforward. The fact that the catalytic activity of nanoceria has been reported under very distinct conditions of pH, ionic strength, NP size and/or concentration hinders the direct comparison between the reported data. Indeed, it depends on the particular testing conditions. Here, when comparing nanoceria and laccase, it is clearly shown that under some conditions, nanoceria is a chemical reagent with oxidizing capacity. Accordingly, the reaction transforms the insoluble Ce^{4+} ions into soluble Ce^{3+}, consuming nanoceria. When NPs are in excess with respect to the substrate, enzymes and NPs appear to behave similarly, which is illusory. It is also worth noting that we proved the robustness of nanoceria after many measurements over a month without much controlling the storage conditions. Therefore, it can also be stated that nanoceria has outstanding reproducibility and stability, thanks to the robustness of inorganic nanomaterials in front of protein structures like enzymes. Finally, we would like to point out that the $Ce^{3+/4+}$ ratio in a nanoceria NP has been easily estimated by titration with ferrocyanide, a procedure that could become a rapid assessment tool for the evaluation of nanoceria in liquid environments. Normally, the determination of the Ce^{3+}/Ce^{4+} ratio is achieved by X-ray photoelectron spectroscopy (XPS)[26] and eventually electron magnetic resonance (EPR);[27] however, these techniques are complex and costly.

This is relevant in the field of biotechnology and biological enzymes and their outstanding specificity and high catalytic activity.[28–30] Since they present intrinsic limitations due to their proteic nature[31] making their catalytic performance susceptible to temperature, ionic concentration, and the electrostatic environment where they operate.[32] Additionally, they are costly and require careful handling due to intrinsic performance variability, all in all pushing for the search for technological alternatives.[33] In this context, nanoparticle oxides may overcome many of the limitations of natural enzymes and contribute to developments in drug development, diagnosis and therapy, food processing and preservation, and bioremediation applications.

Experimental

Synthesis of nanoceria

Nanoceria was synthesized by a hydrothermal method based on the basic precipitation of $CeNO_3$ in the presence of SC. In detail, a TMAOH solution (50 mL, 50 mM) was added to a 50 mL solution containing $CeNO_3$ (20 mM) and sodium citrate (40 mM). The final concentrations were 25 mM TMAOH, 10 mM $CeNO_3$, and 20 mM SC. The reaction mixture was left under stirring overnight at room temperature. Later, the mixture was transferred to a three-necked round bottom flask (250 mL) and left under refluxing at 100 °C for 4 hours. The resulting mixture was a stable, well-dispersed solution of 3.5 nm CeO_2 NPs at a concentration of 1.72 mg mL^{-1} CeO_2.

Citrate 100 mM buffer preparation

Citrate buffer at pH = 4.4 was prepared by mixing 0.2 M citric acid solution (Panreac), 0.2 M sodium citrate solution (Probus) and deionized water in a ratio of 28 : 23 : 49.

Scanning transmission electron microscopy (STEM)

CeO_2 NPs were visualized using STEM (Tecnai F20 S/TEM). 10 μL of the as-synthesized solutions were drop-cast onto a carbon-coated 200 mesh copper grid and left to dry for at least 24 h in the air at room temperature. The average diameter and diameter distribution of the samples were measured using Image Analysis software by counting at least 2000 particles.

UV-visible spectra

UV-vis spectra were acquired with a Cary 60 spectrophotometer (Agilent) using 1.5 mL plastic cuvettes ranging from 250 nm to 800 nm.

Dynamic light scattering

A Malvern ZetaSizer Ultra (Malvern Instruments, UK) operating at a light source wavelength of 532 nm and a fixed scattering angle of 173° was used to measure the hydrodynamic size of CeO_2 NPs. Measurements were conducted in 1 cm path cell and at 25 °C.

Inductively coupled plasma mass spectrometry (ICPMS)

The levels of elemental cerium were analyzed using ICPMS (7900 ICPMS, Agilent) in *Servei d'Anàlisi Química* (UAB, Barcelona). In brief, samples were centrifuged with 3 kDa centrifugal filter units (Amicon-Ultra-15, Merck, Germany) in order to separate ionic dissolved cerium from the NP fraction. Thereafter, microwave assisted digestion (Metrohm, Milestone Ethos Easy, Milestone Systems, Denmark) using HNO_3 at 200 °C was performed.

Kinetic studies for laccase enzyme and nanoparticles with ferricyanide as a substrate

A 96-well plate (flat bottom, 400 μL per well, Sigma-Aldrich) was used to perform an optical inspection of the redox reaction. The columns were filled with consecutive half-dilutions of the enzymes and nanoparticles starting from a concen-

 This journal is © The Royal Society of Chemistry 2022

Open Access Article. Published on 19 August 2022. Downloaded on 7/19/2025 7:26:35 AM.
This article is licensed under a Creative Commons Attribution-NonCommercial 3.0 Unported Licence.

tration of 0.1 mg mL^{-1} for the least active laccase (L1, laccase from *Trametes versicolor* purchased from Sigma-Aldrich EC 1.10.3.2, reference 38429), 0.01 mg mL^{-1} for the most active laccase (L2, laccase from *Trametes versicolor* purchased from Sigma-Aldrich EC 1.10.3.2, reference 51639) and 0.4 mg mL^{-1} for both the commercial (PlasmaChem, cerium oxide nanoparticles, 5 wt% aqueous suspension, average diameter size of 4 nm) and synthesized NPs (average diameter size of 3.5 nm). Citrate buffer (adjusted to pH 4.4) was used as the medium and solvent for the solution preparations. Potassium ferricyanide ($K_3[Fe(CN)_6]$, Sigma-Aldrich) was added to the wells at a final concentration of 1 mM to start the chemical reaction. Kinetic measurements were performed with an ELISA plate reader (Varioskan Flash from Thermo Scientific) at a wavelength of 420 nm every 30 seconds for over an hour. Note that an initial incubation time of 2 min was needed in order to fill all the wells of the plate with the ferricyanide solution (this initial time is included in the graphs).

X-ray diffraction analysis of nanoceria

X-ray diffraction (XRD) data were collected on a PANalytical X'Pert diffractometer using a Cu Kα radiation source (λ = 1.541 Å). In a typical experiment, the 2θ diffraction (Bragg) angles were measured by scanning the goniometer from 10° to 95°. The samples were prepared by centrifugation to precipitate the NCs. The solutions were centrifuged and dried-out on a vacuum-evaporating chamber for several hours. The powder obtained was compacted and directly analyzed. Peak positions and their full width at half maximum (FWHM) were determined using the X'Pert HighScore program after baseline correction.

Reproducibility and robustness tests

Statistical analysis. The measurements were performed analogously to the ones for the kinetic studies but only the synthesized NPs were tested. The experiments were performed three times over a month: at day 0, day 15 and day 30. The nanoparticles were stored at room temperature, in a transparent glass bottle and not protected from sunlight. The statistical analysis was performed using GraphPad Prism software version 8, considering $p < 0.05$ statistically significant.

Conflicts of interest

There are no conflicts to declare.

Acknowledgements

N. Sabaté would like to acknowledge the financial support received from ERC Consolidator Grant (SUPERCELL – GA.648518). N. G. B and V. P. acknowledge financial support from the Spanish Ministerio de Ciencia, Innovación y Universidades (MCIU) (RTI2018-099965-B-I00, AEI/FEDER,UE) proyectos de I + D + i de programación conjunta internacional MCIN/AEI (CONCORD, PCI2019-103436) cofunded by the European Union and Generalitat de Catalunya (2017-SGR-1431). ICN2 is supported by the Severo Ochoa program from Spanish MINECO (SEV-2017-0706) and is funded by the CERCA Programme/Generalitat de Catalunya. Dmitry Galyamin thanks the doctoral program "Electroquímica. Ciència i Tecnologia" of the Universitat Autònoma de Barcelona (UAB).

Notes and references

1 L. Gao, J. Zhuang, L. Nie, J. Zhang, Y. Zhang, N. Gu, T. Wang, J. Feng, D. Yang, S. Perrett and X. Yan, *Nat. Nanotechnol.*, 2007, **2**, 577–583.
2 J. Wu, X. Wang, Q. Wang, Z. Lou, S. Li, Y. Zhu, L. Qin and H. Wei, *Chem. Soc. Rev.*, 2019, **48**, 1004–1076.
3 H. Wei, L. Gao, K. Fan, J. Liu, J. He, X. Qu, S. Dong, E. Wang and X. Yan, *Nano Today*, 2021, **40**, 101269.
4 S. Scott, H. Zhao, A. Dey and T. B. Gunnoe, *ACS Catal.*, 2020, **10**, 14315–14317.
5 C. Korsvik, S. Patil, S. Seal and W. T. Self, *Chem. Commun.*, 2007, **10**, 1056–1058.
6 J. D. Cafun, K. O. Kvashnina, E. Casals, V. F. Puntes and P. Glatzel, *ACS Nano*, 2013, **7**, 10726–10732.
7 T. Pirmohamed, J. M. Dowding, S. Singh, B. Wasserman, E. Heckert, A. S. Karakoti, J. E. S. King, S. Seal and W. T. Self, *Chem. Commun.*, 2010, **46**, 2736–2738.
8 Y. Yue, H. Wei, J. Guo and Y. Yang, *Colloids Surf., A*, 2021, **610**, 125715.
9 B. Chishti, H. Fouad, H. K. Seo, O. Y. Alothman, Z. A. Ansari and S. G. Ansari, *New J. Chem.*, 2020, **44**, 11291–11303.
10 A. Asati, S. Santra, C. Kaittanis, S. Nath and J. M. Perez, *Angew. Chem.*, 2009, **121**, 2344–2348.
11 S. Singh, *Front. Chem.*, 2019, **7**, 46.
12 L. M. Ernst and V. Puntes, *Front. Immunol.*, 2022, **13**, 750075.
13 N. J. Lawrence, J. R. Brewer, L. Wang, T.-S. Wu, J. Wells-Kingsbury, M. M. Ihrig, G. Wang, Y.-L. Soo, W.-N. Mei and C. L. Cheung, *Nano Lett.*, 2011, **11**, 2666–2671.
14 J. S. P. Cresi, M. Chiara Spadaro, S. D'Addato, S. Valeri, L. Amidani, F. Boscherini, G. Bertoni, D. Deiana and P. Luches, *Nanotechnology*, 2017, **28**, 495702.
15 V. Seminko, P. Maksimchuk, O. Avrunin, V. Semenets and Y. Malyukin, *Phys. Status Solidi B*, 2019, **256**, 1900325.
16 L. C. Zhao, M. H. Guo, X. D. Li, Y. P. Huang, S. H. Wu and J. J. Sun, *Anal. Chem.*, 2017, **89**, 13429–13433.
17 E. K. Goharshadi, S. Samiee and P. Nancarrow, *J. Colloid Interface Sci.*, 2011, **356**, 473–480.
18 D. Banham, S. Ye, T. Cheng, S. Knights, S. M. Stewart, M. Wilson and F. Garzon, *J. Electrochem. Soc.*, 2014, **161**, F1075–F1080.
19 Y. P. Lan and H. Y. Sohn, *Mater. Res. Express*, 2018, **5**, 035501.

Open Access Article. Published on 19 August 2022. Downloaded on 7/19/2025 7:26:35 AM.
This article is licensed under a Creative Commons Attribution-NonCommercial 3.0 Unported Licence.

20 M. Pourbaix, *Atlas of Electrochemical Equilibria in-Aqueous Solutions*, Pergamon Press, Oxford, New York, 1966.
21 F. Schwabe, R. Schulin, P. Rupper, A. Rotzetter, W. Stark and B. Nowack, *J. Nanopart. Res.*, 2014, **16**, 2668.
22 F. Lemont and A. Barbier, *Hydrometallurgy*, 2019, **183**, 193–198.
23 K. Reed, A. Cormack, A. Kulkarni, M. Mayton, D. Sayle, F. Klaessig and B. Stadler, *Environ. Sci. Nano*, 2014, **1**, 390–405.
24 H. Cheng, S. Lin, F. Muhammad, Y. W. Lin and H. Wei, *ACS Sens.*, 2016, **1**, 1336–1343.
25 P. Ni, X. Wei, J. Guo, X. Ye and S. Yang, *RSC Adv.*, 2015, **5**, 97512–97519.
26 X. Xia, Y. Lan, J. Li, C. Chen, B. Xu, X. Luo and X. Mao, *J. Rare Earths*, 2020, **38**, 951–960.
27 R. M. Rakhmatullin, V. V. Semashko, S. L. Korableva, A. G. Kiiamov, A. A. Rodionov, R. Tschaggelar, J. A. van Bokhoven and C. Paun, *Mater. Chem. Phys.*, 2018, **219**, 251–257.
28 A. S. Bommarius and M. F. Paye, *Chem. Soc. Rev.*, 2013, **42**, 6534–6565.
29 H. Rastogi and S. Bhatia, in *Enzymes in Food Biotechnology: Production, Applications, and Future Prospects*, Elsevier, 2018, pp. 845–860.
30 S. K. Metkar and K. Girigoswami, *Biocatal. Agric. Biotechnol.*, 2019, **17**, 271–283.
31 R. Assis and A. S. Kondrashov, *Mol. Biol. Evol.*, 2014, **31**, 419.
32 L. J. Jensen, D. W. Ussery and S. Brunak, *Genome Res.*, 2003, **13**, 2444–2449.
33 G. F. D. Del Castillo, M. Koenig, M. Müller, K. J. Eichhorn, M. Stamm, P. Uhlmann and A. Dahlin, *Langmuir*, 2019, **35**, 3479–3489.

This journal is © The Royal Society of Chemistry 2022